

Magnetic-Induced-Piezopotential Gated MoS₂ Field-Effect Transistor at Room Temperature

Yudong Liu, Junmeng Guo, Aifang Yu, Yang Zhang, Jinzong Kou, Ke Zhang, Rongmei Wen, Yan Zhang, Junyi Zhai,* and Zhong Lin Wang*

Utilizing magnetic field directly modulating/turning the charge carrier transport behavior of field-effect transistor (FET) at ambient conditions is an enormous challenge in the field of micro–nanoelectronics. Here, a new type of magnetic-induced-piezopotential gated field-effect-transistor (MIPG-FET) base on laminate composites is proposed, which consists of Terfenol-D, a ferroelectric single crystal (PMNPT), and MoS₂ flake. When applying an external magnetic field to the MIPG-FET, the piezopotential of PMNPT triggered by magnetostriction of the Terfenol-D can serve as the gate voltage to effectively modulate/control the carrier transport process and the corresponding drain current at room temperature. Considering the two polarization states of PMNPT, the drain current is diminished from 9.56 to 2.9 μA in the P_{up} state under a magnetic field of 33 mT, and increases from 1.41 to 4.93 μA in the P_{down} state under a magnetic field of 42 mT and at a drain voltage of 3 V. The current on/off ratios in these states are 330% and 432%, respectively. This work provides a novel noncontact coupling method among magnetism, piezoelectricity, and semiconductor properties, which may have extremely important applications in magnetic sensors, memory and logic devices, micro-electromechanical systems, and human–machine interfacing.

Multifield coupling devices are the devices coupled with two or more basic physical fields, which have broad applications in sensors, information storage, and human–computer interfacing.^[1–3] With the rapid development of electronic and communication technology, the miniaturization and integration of electronic element demands new multifunctional materials, especially magnetic and semiconductor materials. Though researchers' attempt to combine the characteristics of both materials to develop a new generation of electronic devices, such as doping magnetic elements into semiconductors, there has been little important progress in the integration of magnetic materials and semiconductor,^[4] whether in basic research or industrial applications. Semiconductor spintronics,^[5] as an interdisciplinary bridging microelectronics and magnetism, has drawn much attention in the past few years. However, the spin-dependent transport usually need the extreme condition including low temperature and high mag-

netic field, which may be a huge obstacle to practical applications of the spintronic devices.^[6] Therefore, it is extraordinarily necessary to explore and design suitable coupling materials for electronic devices at general condition. However, realizing the perfect coupling between magnetism and semiconductor in single-phase material is very hard and usually requires extreme working condition. So, experimentally preparing the composite devices that couple magnetism and semiconductor at room temperature has terribly important significance.

Recently, 2D atomically thin transition metal dichalcogenides such as MoS₂, WS₂, and MoTe₂ have gained extensive concerning due to their unique electronic, optical, photocatalytic,^[7] and piezoelectric properties.^[8,9] The bulk MoS₂ is a typical semiconductor with an indirect bandgap of 1.2 eV, while the monolayer MoS₂ possesses a large intrinsic direct bandgap of 1.8 eV. As a result, single-layer MoS₂ could be complementary to zero-bandgap graphene in electronic applications, such as field-effect transistors,^[10] piezotronic transistor,^[11] phototransistor^[12,13] and energy harvester.^[14] Field-effect transistors with single-layer MoS₂ flake as conductive channel have displayed many outstanding features, such as exceptionally high current on/off ratio of 10⁷–10⁸ at room temperature and low subthreshold swing of 74 mV decade⁻¹.^[15] However, all of

Y. Liu, J. Guo, Dr. A. Yu, Dr. Y. Zhang, J. Kou, K. Zhang, R. Wen, Prof. Y. Zhang, Prof. J. Zhai, Prof. Z. L. Wang
Beijing Institute of Nanoenergy and Nanosystems
Chinese Academy of Sciences
Beijing 100083, P. R. China
E-mail: jyzhai@binn.cas.cn; wang@mse.gatech.edu

Y. Liu, J. Guo, Dr. A. Yu, Dr. Y. Zhang, J. Kou, K. Zhang, R. Wen, Prof. Y. Zhang, Prof. J. Zhai, Prof. Z. L. Wang
CAS Center for Excellence in Nanoscience
National Center for Nanoscience and Technology (NCNST)
Beijing 100190, P. R. China

Y. Liu, J. Guo, J. Kou, K. Zhang, R. Wen
University of Chinese Academy of Sciences
Beijing 100049, P. R. China

Prof. Y. Zhang
State Key Lab Elect Thin Films and Integrated Devices
University of Electronic Science and Technology of China
Chengdu 610054, P. R. China

Prof. Z. L. Wang
School of Materials Science and Engineering
Georgia Institute of Technology
Atlanta, GA 30332, USA

 The ORCID identification number(s) for the author(s) of this article can be found under <https://doi.org/10.1002/adma.201704524>.

DOI: 10.1002/adma.201704524

these known electronic devices are almost stimulated by electric field. Ferroelectric materials, such as polyvinylidene fluoride-trifluoroethylene and lead zirconium titanate ($\text{Pb}(\text{Zr,Ti})\text{O}_3$), have been employed to integrate with 2D semiconductor materials (MoS_2 , WSe_2) to form negative capacitance field-effect transistors^[16–18] or ferroelectric field-effect transistor (FeFET) for memory and logic devices.^[19] In these devices, the roles of the ferroelectric materials act as gate dielectric by controlling their remnant polarization to tune the density of carriers in FeFET and fulfill on and off states.^[20] This idea provides an innovative and effective coupling method by tuning the conductive channel of 2D materials through field-induced charges at the interface instead of traditional electric field.^[21–23]

In contrast with the modulation of carrier transport characteristic by electric field or charges, few works are reported by other common methods, i.e., magnetic field. In this paper, we demonstrate a novel multifield coupled magnetic-induced-piezopotential gated field-effect transistor (MIPG-FET), which is composed of rare-earth Terfenol-D ($\text{Tb}_x\text{Dy}_{(1-x)}\text{Fe}$ alloys), ferroelectric single crystal $[\text{Pb}(\text{Mg}_{1/3}\text{Nb}_{2/3})\text{O}_3]_{(1-x)}[\text{PbTiO}_3]_x$ (PMNPT), and 2D MoS_2 flake. The noncontact MIPG-FET can realize the modulation of carrier transport property in MoS_2 channel via low magnetic field through PMNPT/Terfenol-D composite at room temperature. With giant magnetostriction coefficient, the rare-earth Terfenol-D can provide a stable tensile strain or stress under external magnetic field. The ferroelectric single crystal PMNPT has giant piezoelectric constant and electromechanical coupling coefficient, which could produce sufficient polarization charges on the surface under applied

strain. The monolayer MoS_2 flake is utilized as conductive channel in the MIPG-FET. Compared with conductive channel of 3D semiconductor materials, the atomically thick channel of 2D MoS_2 flake is more easily controlled by gate voltage or the polarization charges. When a magnetic field is applied to the MIPG-FET, the Terfenol-D will be elongated. The stable strain transition from Terfenol-D will generate a fixed number of polarization charges at the interface of PMNPT and then modulate/turn the carrier transport in MoS_2 channel instead of traditional external gate voltage. In particular, the channel material of the MIPG-FET is not just limited to the MoS_2 flake, other 2D semiconductor materials are also available. The multifield coupling device based on laminate composites is systematically examined and may inspire many potential applications in micro-electromechanical systems (MEMS), sensors, and non-contact detection.

Figure 1a summarizes the three-phase coupling effects among magnetism, semiconductor, and piezoelectricity, in which involves two-phase coupling effects (piezotronic, spintronic, and magnetoelectric effect) and three-phase coupling effects (magneto-piezotronics). Piezotronics were first proposed in 2007,^[24–27] which use the inner crystal piezopotential as a “gate” voltage to tune/control the carrier transport at the interface of metal/semiconductor contacts or semiconductor heterojunctions.^[28–32] Spintronics as a bridge connecting magnetism and semiconductor aims at studying how to manipulate the spin-polarized current.^[33,34] Magnetoelectric effect is the phenomenon of inducing magnetic (electric) polarization by applying an external electric (magnetic) field,^[35] which was

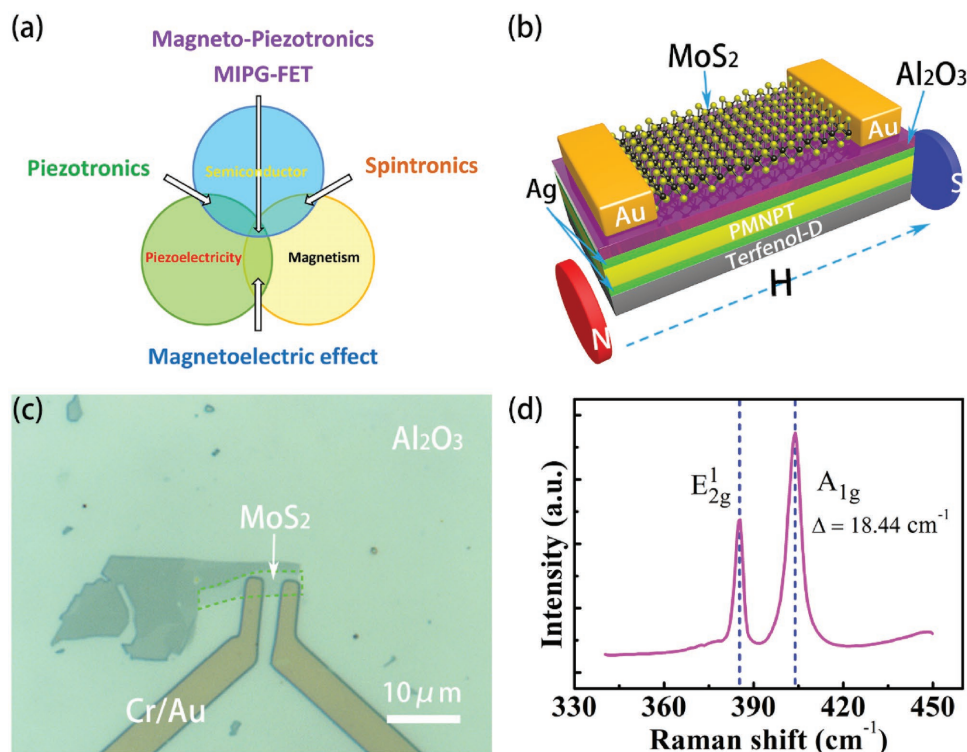


Figure 1. Relation of the three-phase coupling system and the structure of MIPG-FET as well as characterization of the MoS_2 flake. a) Schematic diagram showing the three-phase coupling among magnetism, semiconductor, and piezoelectricity. b) 3D schematic illustration of an MoS_2 -based MIPG-FET. c) Optical image of a typical MoS_2 transistor on PMNPT. d) Raman spectrum of the MoS_2 flake shown in (c).

first prophesied by Curie in 1894.^[36] However, the magneto-piezotronics is a relatively complex system, which involves three-phase coupling among magnetism, semiconductor, and piezoelectricity and has not yet been explored so far. Fortunately, the laminate composite MIPG-FET provides an equivalent conversion method to realize the multifield couplings effect mentioned above.

The basic structure of the MIPG-FET consists of Terfenol-D, PMNPT, and monolayer MoS₂ flake, as schematically shown in Figure 1b. The dimension of high-quality single crystal PMNPT (001) with double side polished was 10 × 5 × 0.5 mm³. First, Cr and Ag were successively deposited on both sides of PMNPT as bottom and top electrodes. Then, a 60 nm Al₂O₃ layer was deposited on the top electrode (back gate) by atomic layer deposition as an insulating and dielectric layer. The monolayer MoS₂ flake was transferred to the top of Al₂O₃ layer. Owing to the van der Waals forces, the MoS₂ flake was tightly attached to the surface of Al₂O₃. Source and drain electrodes were fabricated on MoS₂ flake using electron-beam lithography followed by evaporation of Cr and Au. At last, the PMNPT substrate with MoS₂ transistor was tightly bonded with the bulk Terfenol-D using hard epoxy resins and then was put in glove box for 24 h (for more details see Figure S1 of the Supporting Information). As we can see from the optical microscopy image of a typical device in Figure 1c, the conductive channel between the source and drain is about 2.5 μm, connected by MoS₂ flake, and the channel width is also around 2.5 μm. Figure 1d shows Raman spectrum of the MoS₂ flake used in Figure 1c. The spectrum reveals that the distance between the in-plane E_{2g}¹ mode and out-of-plane A_{1g} mode is 18.44 cm⁻¹, which indicates the MoS₂ flake in the device is monolayer.^[37] The ferroelectric hysteresis loop of PMNPT and the magnetostriction of Terfenol-D are shown in Figures S2 and S3 of the Supporting Information, respectively.

We first characterized the basic electrical performances of the back gate MIPG-FET without applying external magnetic field, in which the top electrode of the PMNPT served as back gate and two gold electrodes acted as the source and drain, with source grounded. The cross-section view of the MIPG-FET structure and the corresponding connection configuration are shown in Figure 2a. All electrical measurements were performed by a Semiconductor Characterization System (Keithley 4200) under ambient environmental condition. The typical output (I_{ds} - V_{ds}) and transfer (I_{ds} - V_{gs}) curves are shown in Figure 2b,c, respectively. The drain current (I_{ds}) increases linearly with the

increase in the gate voltage varying from 0 to 2 V due to the accumulation of the electrons in the MoS₂ channel, which indicates that the MoS₂ presents a typical n-type behavior, in accordance with previous reports.^[38] The obtained on/off ratio of the MoS₂ transistor is about 10⁶ from the transfer curve, which is comparable to the former reports.^[15] Meanwhile, we notice that the I_{ds} - V_{ds} characteristic (at zero gate voltage) showed nonlinear behavior in the ±3 V range of voltage, manifesting that the contacts between gold and MoS₂ flake were not Ohmic contacts but Schottky contacts with certain barrier height. This may attribute to absorption of oxygen and water from the environment during transfer process,^[39] which may degrade the performance of the device. But it will not affect the discussion of physical mechanism of the MIPG-FET. Moreover, the out curves were not saturates due to the high contact resistance from Schottky barrier hindering the transmission of electrons.^[40]

Next, the magnetic-modulated response of the MIPG-FET was systematically characterized. In view of the ferroelectric property of the PMNPT, we need to consider three different states of MIPG-FET: without electrical polarization (the original state), polarization up (P_{up}) state, and polarization down (P_{down}) state. The P_{up} and P_{down} states can be achieved by poling PMNPT (0.5 mm in thickness) with -400 and +400 V, respectively. To begin with, we discussed the P_{up} state. The I_{ds} - V_{ds} output characteristics of the original and P_{up} states (at zero gate voltage) are shown in Figure 3a. Compared with the original state, the drain current is obviously enhanced in the P_{up} state due to the remnant polarization of the PMNPT after polarization accumulating the carriers in the MoS₂ channel^[41] (as discussed in detail below). Figure 3b shows the magnetic field dependence of I_{ds} output response of the MIPG-FET without additional gate voltage. It can be seen that the drain current is decreased gradually with the increase in the magnetic field, which is equal to applying an externally decreased voltage to the back gate. The experiment data manifest that the magnetic-induced piezopotential could effectively serve as gate voltage to tune/modulate charge carrier transport in the MoS₂ channel. Figure 3c shows the drain current (derived from Figure 3b) as a function of the magnetic field at a drain voltage of 3 V. With the magnetic field increasing from 0 to 33 mT, the drain current diminished from 9.56 to 2.9 μA, approximately for 330%, presenting a monotonically decreasing tendency. The drain current I_{ds} with different magnetic fields versus time and the transient response of the MIPG-FET (under $V_{ds} = 3$ V) are respectively

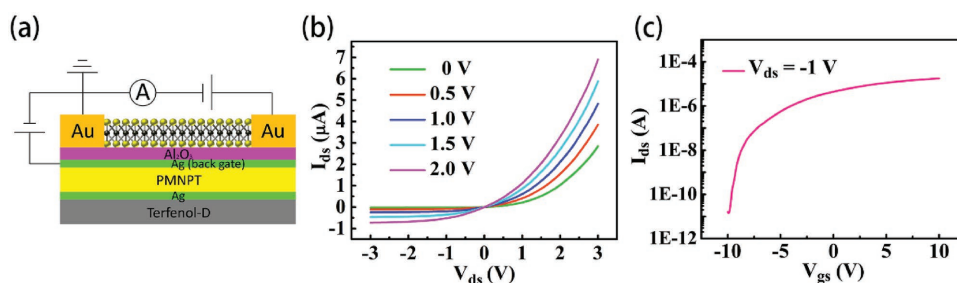


Figure 2. Basic electrical characterization of back gate MoS₂ transistor of the MIPG-FET with an external gate voltage. a) Cross-section view of the MIPG-FET as well as the corresponding electrical connections used to characterize the MoS₂ transistor. b) Output characteristics I_{ds} - V_{ds} with different back gate voltages. c) Transfer characteristics I_{ds} - V_{gs} with the applied bias voltage V_{ds} of -1 V.

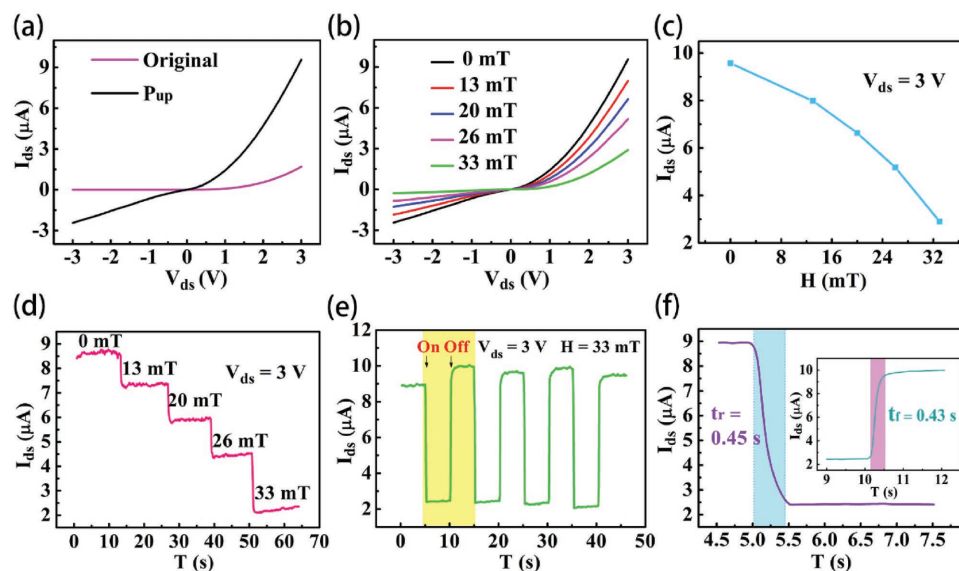


Figure 3. Characteristics of the MIPG-FET in the P_{up} state (at zero gate voltage). a) The I_{ds} - V_{ds} characteristics with the original and P_{up} states of PMNPT. b) I_{ds} - V_{ds} output characteristics with different magnetic fields. c) The drain current as a function of the magnetic field at a drain bias of 3 V. d) I_{ds} output characteristics with different magnetic fields versus times. e) Transient response of the MIPG-FET at $H = 33$ mT, $V_{ds} = 3$ V. f) The rise and fall times of the drain current of the MIPG-FET.

shown in Figure 3d,e, which indicate that the magnetic field presents switch behavior and the current on/off ratio is about 330% in this state. The on/off ratio and the sensitivity can be further improved by reducing the thickness of insulating layer or choosing other high- k material as the gate dielectric layer, and by using larger magnetostriction materials such as metallic glass. The applied magnetic field used in this measurement was low, which could be generated by multiferroic heterostructure in low energy consumption.^[42] To explore the response time of the MIPG-FET, we enlarged a complete on/off cycle as shown in Figure 3e. The trigger time (“rise” time, t_r) and recovery time (“fall” time, t_f) of the drain current are about 0.45 and 0.43 s (as shown in Figure 3f), respectively. It should be noted that the rising time is just the response time of the MIPG-FET, which is relevant to the permittivity and thickness of the gate insulator, magnetostrictive coefficient and response rate of Terfenol-D, piezoelectric constants of PMNPT, coupling factor between the Terfenol-D and PMNPT, and so on. They also could be enhanced by selecting appropriate materials with their best performances. These experiment results demonstrate that the MIPG-FET has successfully realized perfect coupling between magnetism and semiconductor at low magnetic field (33 mT), which may derive plenty of potentially important applications in magnetic sensors and actuators, information storage devices, and noncontact detection system.

Then, we investigated characteristics of the MIPG-FET in the polarization down state of PMNPT. On the contrary to the P_{up} state, the drain current in the P_{down} state is much smaller than that of the original state, as shown in Figure 4a. This is because of depletion of the intrinsic carriers in the MoS_2 channel caused by remnant polarization of PMNPT. The I_{ds} - V_{ds} output characteristics with different magnetic fields from 0 to 42 mT and the drain current versus applied magnetic field ($V_{ds} = 3$ V) are illustrated in Figure 4b,c, respectively. In contrast

to the P_{up} state, the drain current in the P_{down} state is increased monotonically with increasing magnetic field, and the effect of the applied magnetic field is equivalent to an externally positive gate voltage. Figure 4d shows the transient characteristics of the MIPG-FET in the P_{down} state. The on/off ratio is about 432% in this case, which is roughly the same as the data in the P_{up} state. The cyclical variations of the drain current at a periodically applied magnetic field of 42 mT show that the device exhibits a high degree of repeatability. These results suggest that the magnetic field can also replace the external gate voltage to control the carrier transport behavior in this state, while the drain current presents an opposite variation tendency compared with the P_{up} state.

To further investigate the physical mechanism of how the magnetic field turns the carrier transport property in MIPG-FET, two physical effects (magnetoresistance effect and piezoresistance effect in MoS_2) should be taken in account. To rule out the influence of magnetoresistance, we fabricated the similar MoS_2 flake FET on PMNPT without Terfenol-D. In this case, the drain current did not change with the applied external magnetic field (Figure S4 of the Supporting Information). Then, Raman spectrum was used to examine the influence of the piezoresistance effect, and the results showed that there were no changes in the distance between the in-plane E_{2g}^1 mode and the out-of-plane A_{1g} mode of the MoS_2 flake in MIPG-FET with and without applied magnetic field of 42 mT (Figure S5 of the Supporting Information). In fact, the strain from Terfenol-D was too small to change Raman spectrum or bandgap of MoS_2 .^[43,44] Therefore, it is confirmed that the opposite changes of the drain current of MIPG-FET in two different polarized states under magnetic field are only caused by the piezopotential of PMNPT induced by the magnetic field.

In order to minutely illuminate the working principle of the MIPG-FET, and how it couples the magnetism, piezoelectricity,

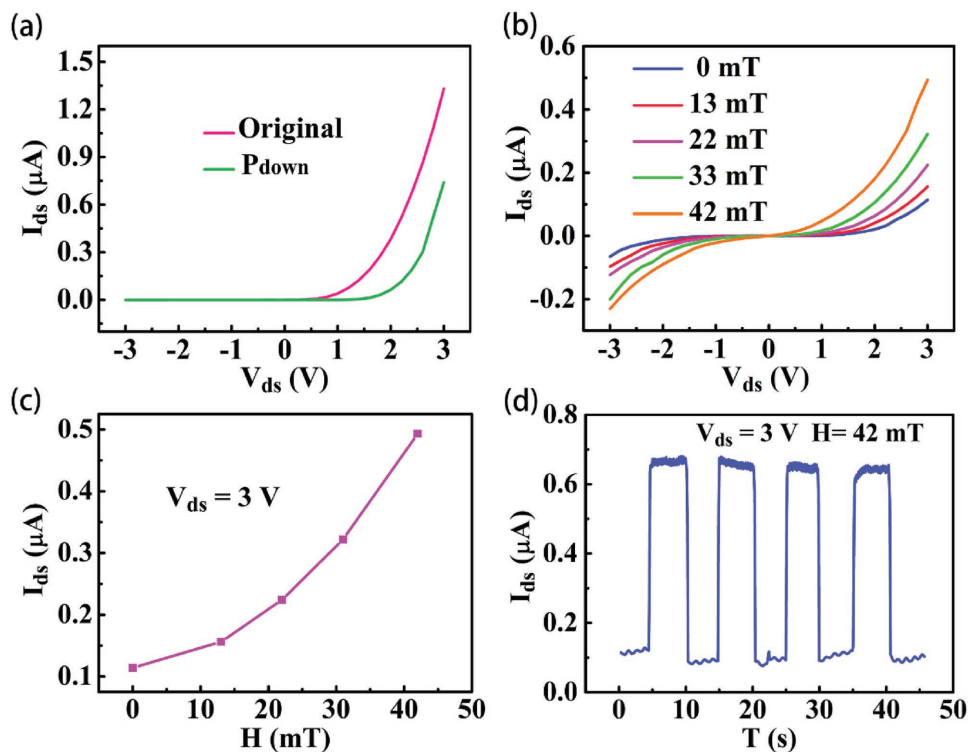


Figure 4. Characteristics of MIPG-FET in the P_{down} state (at zero gate voltage). a) The $I_{\text{ds}}-V_{\text{ds}}$ characteristics with the original and P_{down} states of PMNPT. b) $I_{\text{ds}}-V_{\text{ds}}$ output characteristics with different magnetic fields. c) Magnetic field dependence of the drain current at a drain bias of 3 V. d) The transient characteristics of the MIPG-FET under the magnetic field of 42 mT and the drain bias of 3 V.

and semiconductor, we raise schematic band diagrams of the laminate composites to interpret the piezopotential effect on the devices before and after applying the magnetic field, as shown in Figure 5. The architecture of MIPG-FET is vertically built by stacking Terfenol-D, PMNPT, and MoS_2 flake, and the cross-section and initial band diagram are shown in Figure 5a. In the original state, electric dipoles in the PMNPT are randomly distributed and there are no net polarization charges forming on the surface, so they have no influence on the carrier density and conductive channel width of MoS_2 . After we poled the PMNPT by negative electric field (-400 V), the dipoles would align vertically along the thickness direction, leaving net positive and negative polarization charges in the upper and lower surfaces of PMNPT due to the remnant polarization, respectively. At the same time, an equal number of positive and negative electrostatic charges would homogeneously generate and distribute in both the metal electrodes to balance the polarization charges owing to electrostatic induction, as shown in Figure 5b (top). As a result, there exist net unscreened positive electrostatic charges on the upper surface of the top metal electrode (back gate), which could produce a positive inner electric field across back gate and the grounded source electrode. The inner electric field can accumulate the free carriers of MoS_2 channel (bottom of Figure 5b)^[45] and then cause the drain current much larger than that of the original state, consistent with Figure 3a. When the MIPG-FET was exposed to an external magnetic field, Terfenol-D would produce tensile strain. The strain would transfer to PMNPT through hard epoxy interlayer, resulting in partial reduction of polarization charges because

of the piezoelectric effect (top of Figure 5c). Therefore, the net unscreened positive electrostatic charges decreased as well and the ability to accumulate carriers weakened. It was to reduce the carrier density in the MoS_2 channel (bottom of Figure 5c) and the corresponding drain current (Figure 3b), similar to applying an external negative gate voltage on the back gate. This is why the drain current I_{ds} decreased gradually with the increase in the applied magnetic field. On the contrary, in the P_{down} state, there would be net negative polarization charges in the upper surface of the PMNPT and matching amount of unscreened inductively negative charges on the top metal electrode after a voltage of $+400$ V was imposed (top of Figure 5d). They would cause the depletion of the charge carriers in the MoS_2 channel (bottom of Figure 5d) and then apparently diminish the drain current compared with the original state (Figure 4a). Once the external magnetic field was applied, the net negative polarization charges and inductively unscreened negative charges would lessen simultaneously (top of Figure 5e). This would bring about the ability to deplete carrier lessening, and produce gradual increase in carriers in the MoS_2 channel and the drain current (bottom of Figure 5e), showing a reverse trend to that in the P_{up} state (Figure 4b). Under this condition, the external magnetic field acted as a positive gate voltage for MIPG-FET.

To summarize, we have fabricated a multifield coupled magnetic-induced-piezopotential FET, in which the MoS_2 flake, easily accumulated and depleted due to atomically thin layer, was selected as conductive channel and the piezopotential of PMNPT triggered by magnetic field worked as a gate. With the successful coupling of the magnetism, piezoelectricity,

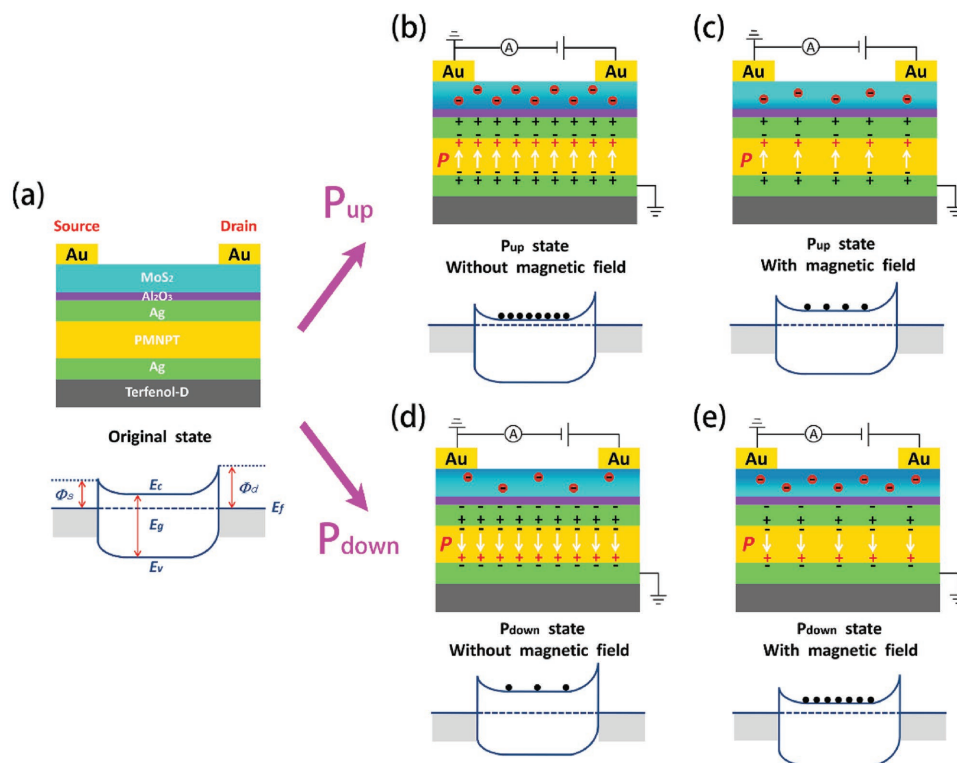


Figure 5. Schematic working principle of the MIPG-FET in three states (at zero gate voltage). a) The cross section (top) and initial band diagram (bottom) of the MIPG-FET without magnetic field. b,c) The cross-section structures of the device and equilibrium energy band diagrams of the P_{up} state with and without magnetic field. d,e) The cross-section structures of the device and equilibrium energy band diagrams of the P_{down} state with and without magnetic field. E_f , E_c , E_v , E_g , Φ_s , and Φ_d are the Fermi level energy, minimum conduction band energy, maximum valence band energy, bandgap of MoS_2 , and Schottky barrier height of source and drain, respectively.

and semiconductor, the applied magnetic field can effectively modulate the channel carrier transport in the MIPG-FET. Notably, the MIPG-FET can operate at room temperature and low magnetic field, and it does not need extreme conditions. In the P_{up} and P_{down} states of PMNPT, the drain currents changing inversely with magnetic field (monotone increasing or decreasing) manifest that the magnetic field could take the place of the traditional external gate voltage. The on/off ratio in the P_{up} and P_{down} states can reach 330% and 432%, respectively, under external magnetic field as low as 33 or 42 mT. The integrated laminate composite devices offer a new technical route coupling magnetism and semiconductor besides spintronics, and greatly enrich the exploration and application in the piezo-magnetotronics research area, which may be widely employed in magnetic sensor, memory and logic device, MEMS, and non-contact and nondestructive detection. The experiment results prove the feasibility of the multifield coupling device proposed by us. More novel devices and applications based on our study may be explored in the near future.

Experimental Section

Fabrication of the MIPG-FET: The single crystal PMNPT sheets (001) were machined in the dimension of $10 \times 5 \times 0.5 \text{ mm}^3$. Next, a 10 nm Cr and a 100 nm Ag layer were deposited by sputter on both sides as surface electrodes. Then a 60 nm thick layer of high-quality Al_2O_3 was deposited on the top surface electrode by atomic layer

deposition as a gate dielectric and insulating layer. By mechanical exfoliation, the monolayer MoS_2 flake was wet transferred to the Al_2O_3 layer using poly (methyl methacrylate) and 5% aqueous solution of hydrofluoric acid. After transfer process, 10 nm Cr and 50 nm Au were successively fabricated using electron-beam lithography as source and drain electrodes. And then the PMNPT were polarizing by high voltage supply under -400 and $+400$ V for 20 min, respectively. Finally, the PMNPT substrate and Terfenol-D with a dimension of $10 \times 5 \times 1 \text{ mm}^3$ were tightly bonded together using hard epoxy resins, and the final devices were placed in a glove box for 24 h to ensure that the epoxy fully cure. All the electrical measurements were carried out using a Keithley semiconductor parameter analyzer (4200) under general conditions. The magnetic field was applied along the longitudinal orientation of the laminate composites and measured by a digital Gauss/Tesla meter.

Supporting Information

Supporting Information is available from the Wiley Online Library or from the author.

Acknowledgements

This work was supported by NSFC 51472056, National Key R&D Project from Minister of Science and Technology, China (Grant Nos. 2016YFA0202703 and 2016YFA0202704), the "thousands talents" program for pioneer researcher and his innovation team, China, and the Recruitment Program of Global Youth Experts, China.

Conflict of Interest

The authors declare no conflict of interest.

Keywords

field-effect transistors, magnetic field, MoS₂ flakes, piezopotential, polarization states

Received: August 10, 2017
Revised: November 18, 2017
Published online:

-
- [1] M. C. Wong, L. Chen, M. K. Tsang, Y. Zhang, J. Hao, *Adv. Mater.* **2015**, *27*, 4484.
- [2] M. Peng, Y. Zhang, Y. Liu, M. Song, J. Zhai, Z. L. Wang, *Adv. Mater.* **2014**, *26*, 6767.
- [3] S. Dong, J.-F. Li, D. Viehland, *Appl. Phys. Lett.* **2003**, *83*, 2265.
- [4] H. Ohno, *Science* **1998**, *281*, 951.
- [5] D. D. Awschalom, M. E. Flatte, *Nat. Phys.* **2007**, *3*, 153.
- [6] S. A. Wolf, D. D. Awschalom, R. A. Buhrman, J. M. Daughton, S. von Molnar, M. L. Roukes, A. Y. Chtchelkanova, D. M. Treger, *Science* **2001**, *294*, 1488.
- [7] J. M. Wu, W. E. Chang, Y. T. Chang, C. K. Chang, *Adv. Mater.* **2016**, *28*, 3718.
- [8] H. Zhu, Y. Wang, J. Xiao, M. Liu, S. Xiong, Z. J. Wong, Z. Ye, Y. Ye, X. Yin, X. Zhang, *Nat. Nanotechnol.* **2015**, *10*, 151.
- [9] K. Zhang, M. Peng, W. Wu, J. Guo, G. Gao, Y. Liu, J. Kou, R. Wen, Y. Lei, A. Yu, Y. Zhang, J. Zhai, Z. L. Wang, *Mater. Horiz.* **2017**, *4*, 274.
- [10] S. B. Desai, S. R. Madhvapathy, A. B. Sachid, J. P. Llinas, Q. X. Wang, G. H. Ahn, G. Pitner, M. J. Kim, J. Bokor, C. M. Hu, H. S. P. Wong, A. Javey, *Science* **2016**, *354*, 99.
- [11] W. Wu, L. Wang, Y. Li, F. Zhang, L. Lin, S. Niu, D. Chenet, X. Zhang, Y. Hao, T. F. Heinz, J. Hone, Z. L. Wang, *Nature* **2014**, *514*, 470.
- [12] Z. Y. Yin, H. Li, H. Li, L. Jiang, Y. M. Shi, Y. H. Sun, G. Lu, Q. Zhang, X. D. Chen, H. Zhang, *ACS Nano* **2012**, *6*, 74.
- [13] W. Wu, L. Wang, R. Yu, Y. Liu, S. H. Wei, J. Hone, Z. L. Wang, *Adv. Mater.* **2016**, *28*, 8463.
- [14] J. Feng, M. Graf, K. Liu, D. Ovchinnikov, D. Dumcenco, M. Heiranian, V. Nandigana, N. R. Aluru, A. Kis, A. Radenovic, *Nature* **2016**, *536*, 197.
- [15] B. Radisavljevic, A. Radenovic, J. Brivio, V. Giacometti, A. Kis, *Nat. Nanotechnol.* **2011**, *6*, 147.
- [16] A. Islam Khan, D. Bhowmik, P. Yu, S. Joo Kim, X. Pan, R. Ramesh, S. Salahuddin, *Appl. Phys. Lett.* **2011**, *99*, 113501.
- [17] A. I. Khan, K. Chatterjee, B. Wang, S. Drapcho, L. You, C. Serrao, S. R. Bakaul, R. Ramesh, S. Salahuddin, *Nat. Mater.* **2015**, *14*, 182.
- [18] F. A. McGuire, Y. C. Lin, K. Price, G. B. Rayner, S. Khandelwal, S. Salahuddin, A. D. Franklin, *Nano Lett.* **2017**, *17*, 4801.
- [19] C. Ko, Y. Lee, Y. Chen, J. Suh, D. Fu, A. Suslu, S. Lee, J. D. Clarkson, H. S. Choe, S. Tongay, R. Ramesh, J. Wu, *Adv. Mater.* **2016**, *28*, 2923.
- [20] A. Lipatov, P. Sharma, A. Gruverman, A. Sinitskii, *ACS Nano* **2015**, *9*, 8089.
- [21] R. S. Dahiya, G. Metta, M. Valle, A. Adami, L. Lorenzelli, *Appl. Phys. Lett.* **2009**, *95*, 034105.
- [22] T. Kawasaki, Y. Akiyama, S. Fujita, S. Satoh, *IEICE Trans. Electron.* **1998**, *E81c*, 584.
- [23] Q. Sun, W. Seung, B. J. Kim, S. Seo, S. W. Kim, J. H. Cho, *Adv. Mater.* **2015**, *27*, 3411.
- [24] Z. L. Wang, *Adv. Mater.* **2007**, *19*, 889.
- [25] Z. L. Wang, *Nano Today* **2010**, *5*, 540.
- [26] X. Wen, W. Wu, C. Pan, Y. Hu, Q. Yang, Z. Lin Wang, *Nano Energy* **2015**, *14*, 276.
- [27] Y. Liu, Y. Zhang, Q. Yang, S. Niu, Z. L. Wang, *Nano Energy* **2015**, *14*, 257.
- [28] C. Liu, M. Peng, A. Yu, J. Liu, M. Song, Y. Zhang, J. Zhai, *Nano Energy* **2016**, *26*, 417.
- [29] C. Pan, L. Dong, G. Zhu, S. Niu, R. Yu, Q. Yang, Y. Liu, Z. L. Wang, *Nat. Photonics* **2013**, *7*, 752.
- [30] M. Peng, Y. Liu, A. Yu, Y. Zhang, C. Liu, J. Liu, W. Wu, K. Zhang, X. Shi, J. Kou, J. Zhai, Z. L. Wang, *ACS Nano* **2016**, *10*, 1572.
- [31] F. Xue, L. Chen, J. Chen, J. Liu, L. Wang, M. Chen, Y. Pang, X. Yang, G. Gao, J. Zhai, Z. L. Wang, *Adv. Mater.* **2016**, *28*, 3391.
- [32] Y. Zhang, Y. Liu, Z. L. Wang, *Adv. Mater.* **2011**, *23*, 3004.
- [33] H. Zeng, J. Dai, W. Yao, D. Xiao, X. Cui, *Nat. Nanotechnol.* **2012**, *7*, 490.
- [34] I. Zutic, J. Fabian, S. Das Sarma, *Rev. Mod. Phys.* **2004**, *76*, 323.
- [35] J. Zhai, Z. Xing, S. Dong, J. Li, D. Viehland, *J. Am. Ceram. Soc.* **2008**, *91*, 351.
- [36] P. Curie, *J. Phys. Théor. Appl.* **1894**, *3*, 393.
- [37] H. Li, Q. Zhang, C. C. R. Yap, B. K. Tay, T. H. T. Edwin, A. Olivier, D. Baillargeat, *Adv. Funct. Mater.* **2012**, *22*, 1385.
- [38] S. Kim, A. Konar, W. S. Hwang, J. H. Lee, J. Lee, J. Yang, C. Jung, H. Kim, J. B. Yoo, J. Y. Choi, Y. W. Jin, S. Y. Lee, D. Jena, W. Choi, K. Kim, *Nat. Commun.* **2012**, *3*, 1011.
- [39] L. P. Hao Qiu, Z. Yao, J. Li, Y. Shi, X. Wang, *Appl. Phys. Lett.* **2012**, *100*, 123104.
- [40] R. Koppera, D. Voiry, S. E. Yalcin, B. Branch, G. Gupta, A. D. Mohite, M. Chhowalla, *Nat. Mater.* **2014**, *13*, 1128.
- [41] X. Wang, P. Wang, J. Wang, W. Hu, X. Zhou, N. Guo, H. Huang, S. Sun, H. Shen, T. Lin, M. Tang, L. Liao, A. Jiang, J. Sun, X. Meng, X. Chen, W. Lu, J. Chu, *Adv. Mater.* **2015**, *27*, 6575.
- [42] M. Liu, S. Li, O. Obi, J. Lou, S. Rand, N. X. Sun, *Appl. Phys. Lett.* **2011**, *98*, 222509.
- [43] Y. Wang, C. Cong, C. Qiu, T. Yu, *Small* **2013**, *9*, 2857.
- [44] L. Yang, X. Cui, J. Zhang, K. Wang, M. Shen, S. Zeng, S. A. Dayeh, L. Feng, B. Xiang, *Sci. Rep.* **2014**, *4*, 5649.
- [45] F. Xue, L. Chen, L. Wang, Y. Pang, J. Chen, C. Zhang, Z. L. Wang, *Adv. Funct. Mater.* **2016**, *26*, 2104.